Engineering Spatial Control of Bacterial Organelles

Y Hoang[1†], Pankaj. V. Jadhav [2†], Daniel S. Trettel[3], Rachel E. Dow[1], Seokmu Kwon[4], Kate Matej[5], Jordan A. Byrne[1], Christopher A. Azaldegui[1], Tobias W. Giessen[4], Hualiang Pi[5], Shyamal Mosalaganti[2,4,6,7*], and Anthony G. Vecchiarelli[1*]

[1] Department of Molecular, Cellular, and Developmental Biology, University of Michigan; Ann Arbor, MI 48109, USA

[2] Life Sciences Institute, University of Michigan; Ann Arbor, MI 48108, USA

[3] Los Alamos National Laboratory, Bioscience Division, Microbial and Biome Sciences Group; Los Alamos, NM 87544, USA

[4] Department of Biological Chemistry, University of Michigan; Ann Arbor, MI 48109, USA

[5] Department of Microbial Pathogenesis and Microbial Sciences Institute, Yale University School of Medicine; New Haven, CT 06510, USA

[6] Department of Cell and Developmental Biology, University of Michigan; Ann Arbor, MI 48109, USA

[7] Department of Biophysics, College of Literature, Science, and the Arts, University of Michigan; Ann Arbor, MI 48109, USA

[†] These authors contributed equally

* Correspondence: ave@umich.edu (A.G.V.), mosalaga@umich.edu (S.M.)

Abstract

Bacteria were once thought to lack organelles, but it is now clear they confine cellular reactions using an array of membrane- and protein-based compartments. A central question, however, is how bacterial organelles are organized in the cell, and whether their spatial control can be engineered. Here, we show that a two-protein system (McdAB) that positions carboxysomes-CO_2-fixing organelles found in autotrophic bacteria-can be repurposed to provide programmable spatial control to diverse organelles in *Escherichia coli*. McdAB not only restores proper assembly and positioning of heterologously expressed carboxysomes in *E. coli*, but can also be reprogrammed to spatially organize all other known types of bacterial organelles, including encapsulins, biomolecular condensates, and even membrane-bound organelles. Programmable spatial organization of bacterial organelles establishes a new design principle for synthetic biology, where the location of reactions is as tunable as their content. Our work paves the way for more efficient biocatalysis in engineered microbes.

Cells achieve remarkable control over biochemistry by organizing reactions in space. In bacteria, protein-based microcompartments, encapsulins, and biomolecular condensates, as well as membrane-bound organelles, enable reactions to be concentrated and regulated without the extensive endomembrane systems of eukaryotes. These self-assembling compartments have drawn broad interest as modular building blocks for synthetic biology. Yet, a central challenge limits their utility: when expressed in heterologous hosts such as *Escherichia coli*, the nucleoid acts as a diffusion barrier (*1–4*). As a result, without spatial control, these organelles form nucleoid-excluded aggregates at the cell pole. This asymmetric distribution in the cell results in a loss of faithful inheritance across the cell population, compromising activity and constraining their applications.

To solve this problem, most bacteria encode minimal, self-organizing systems comprised of a positioning ATPase from the partition protein A (ParA) family, along with a partner protein that links the ATPase to its cellular cargo (*5*). Unlike the linear motors and cytoskeletal systems used by eukaryotes, these two-protein positioning modules generate dynamic ATP-driven protein gradients on the nucleoid to spatially distribute a diversity of cellular cargos, including chromosomes, plasmids, protein complexes, and organelles – ensuring their faithful inheritance and robust functions in the cell. This conserved evolutionary strategy across diverse bacteria and cargo types provides a blueprint for engineering a generalizable method for programming spatial control in bacteria.

The most extensively studied bacterial organelle is the carboxysome, a protein-based organelle found in autotrophic bacteria that is responsible for roughly a third of global CO_2-fixation and holds significant promise for biotechnological applications. Carboxysome organization within the cell is mediated by the Maintenance of Carboxysome Distribution (Mcd) system (*6*, *7*). Specifically, McdB binds carboxysomes and induces McdA oscillations along the nucleoid that distribute carboxysomes throughout the cell to ensure faithful inheritance and CO_2-fixation capacity across the cell population. Without McdAB, carboxysomes mislocalize to the cell poles as nucleoid-excluded aggregates, leading to asymmetric inheritance and a rapid loss of both carboxysomes and CO_2-fixation capacity in the population (*6*, *8*, *9*).

The McdAB system is currently the only known minimal and self-organizing positioning system for any protein-based organelle in bacteria. Inspired by its natural anti-aggregation mechanism, we asked whether McdAB could be repurposed to provide synthetic spatial control. Here, we demonstrate that McdAB not only restores proper assembly and positioning of heterologously-expressed carboxysomes in *E. coli*, but also generalizes to diverse organelles, including protein-based encapsulins and condensates, as well as membrane-bound organelles. Through live-cell imaging, super-resolution microscopy, and *in situ* cryo-electron tomography, we show that McdAB transforms disordered and mispositioned aggregates into evenly distributed, dynamic arrays. By enabling modular and reversible spatial organization, McdAB provides a

versatile strategy for engineering the "*where"* of cellular reactions in bacteria and establishes spatial control as a new design axis for microbial synthetic biology and biotechnology.

Results

The McdAB system spatially organizes carboxysomes in E. coli

Carboxysomes are highly efficient CO_2-fixing organelles, and reconstituting them in *E. coli* could transform this industrial microbe into a powerful chassis for sustainable bioproduction. Yet, despite repeated attempts, engineered carboxysomes in *E. coli* remain dysfunctional. Without their native McdAB positioning system, carboxysomes mislocalize to the cell poles and exhibit poor CO_2-fixation activity (*1*, *4*, *10*, *11*). We have previously shown that even in the native autotrophic host, carboxysome mispositioning in the absence of McdAB disrupts cell growth and division (*9*). These findings underscore the importance of spatial organization for carboxysome function. Motivated by this, we set out to reconstitute not only carboxysome assembly but also its distribution system in *E. coli*.

We used the recently developed inducible 'pXpressome' plasmid toolkit to express α-carboxysomes from the chemoautotroph *Halothiobacillus neapolitanus* in *E. coli*. The small subunit of the carbon-fixing Rubisco enzyme (CbbS) was fused to monomeric NeonGreen (mNG) for *in vivo* fluorescence imaging (Fig. 1A) (*4*). As shown by others, large nucleoid-excluded foci were observed at one or both cell poles (Fig. 1A, C, D; Supplementary Fig. 1A-B). But upon co-expression of the McdAB system, carboxysomes were no longer aggregated at the cell poles (Fig. 1B-D; Supplementary Fig. 1A-B). Instead, multiple foci were distributed across the nucleoid region of the cell. Similar results were obtained when Rubisco was fused to mScarlet or mJuniper, confirming that McdAB-mediated carboxysome positioning is independent of the fluorescent tag used (Supplementary Fig. 1C-D).

Having established that McdAB restores carboxysome organization in *E. coli*, we next examined how this positioning system dynamically regulates organelle distribution in growing and dividing *E. coli* cells over time. Cells were classified based on the number and location of foci: "mispositioned" (0–2 polar foci) and "positioned" (≥3 distributed foci). Without McdAB, carboxysome foci remained mispositioned through cell growth and multiple cell divisions (Fig. 1E-F; Supplementary Fig. 1E; Video S1). In contrast, the vast majority of McdAB-expressing cells maintained distributed carboxysome foci (Fig. 1G-H; Supplementary Fig. 1F; Video S1). These results demonstrate that the McdAB system prevents polar aggregation and promotes the even distribution and increased number of α-carboxysome assemblies in *E. coli*.

While fluorescence imaging revealed that McdAB redistributes Rubisco foci across the cell, this approach lacks the necessary spatial resolution to determine whether the observed foci represent correctly assembled carboxysomes. To directly assess the ultrastructure of these assemblies in the bacterial cell, we performed *in situ* cryo-

electron tomography (cryo-ET). Without McdAB, we observed large, disorganized, and tightly packed arrays of carboxysome components at the cell poles within the tomograms (Fig. 1I, Video S2). We also observed that some fully assembled carboxysomes had individual diameters ranging from 80 to 500 nm - the diameter of α-carboxysomes in *H. neapolitanus*, the native host, ranges from 80 to 120 nm (*12*). By contrast, and consistent with the fluorescence data, McdAB-expressing cells displayed fully assembled, properly sized, and unclustered carboxysomes distributed across the nucleoid region of the cell volume (Fig. 1J, Video S2). Strikingly, we also observed in our *in situ* cryo-tomograms carboxysome "partitioning," where the shell appears to invaginate at the midpoint of a larger carboxysome (Supplementary Fig. 1G, white arrowheads), suggesting that McdAB may play a role in carboxysome assembly and size regulation by subdividing oversized structures.

Taken together, these findings provide direct evidence that McdAB is a truly minimal and self-organizing positioning system - requiring only two proteins to distribute carboxysomes in a heterologous host - while simultaneously promoting their structural integrity and proper assembly.

Spatial control of encapsulin nanocompartments

Building on our discovery that McdAB is minimal and self-organizing, we aimed to repurpose it as a versatile spatial regulator for other bacterial organelles. We recently identified an N-terminal peptide of McdB that is necessary and sufficient for McdA interaction (*13*). Here, we sought to develop this McdB peptide into a minimal autonomous positioning tag or "MapTag". By fusing this MapTag to heterologous organelles and co-expressing McdA, we set out to reprogram their distribution in *E. coli*, starting with encapsulins.

While bacterial microcompartments (BMCs) like the carboxysome are large complex structures, encapsulins are much smaller (20-45 nm) and simpler protein-based nanocompartments found in bacteria and archaea (*14*). The shell is composed of one or two self-assembling proteins that tiles around an enzymatic cargo loaded via an encapsulin-specific targeting peptide (TP). Like BMCs, encapsulins compartmentalize reaction pathways to sequester toxic intermediates, store reaction products, and increase pathway efficiency, thus offering strategies for specialized metabolic engineering of microbes. No native positioning system has been identified for encapsulins so far.

The study, design, and application of encapsulins rely on their robust expression and assembly in heterologous hosts like *E. coli*. Previous studies have revealed that encapsulins aggregate when expressed in *E. coli* (*2*). Therefore, these encapsulins are ideal substrates for testing the MapTag. Nevertheless, encapsulins have never been visualized in live cells. To address this gap, we first developed a method for live-cell visualization. We engineered an inducible plasmid that expressed an encapsulin shell

protein fused to the MapTag, along with a fluorescent cargo protein - mNG fused to a TP (Supplementary Fig. 2A). A degron tag (DT) (*15*) was also fused to mNG to promote degradation of any unencapsulated mNG, thereby enhancing the visualization of mNG-filled encapsulins (*15*). Without McdA, the MapTagged encapsulin foci were nucleoid-excluded to one or both cell poles (Fig. 2A, C-D; Supplementary Fig. 2B-C), consistent with previous work (*2*). But when co-expressed with McdA, several encapsulin foci were distributed along the nucleoid (Fig. 2B-D; Supplementary Fig. B-C).

Having shown that the MapTag can disaggregate and distribute encapsulins in *E. coli*, we next visualized this process in real time. MapTagged encapsulins remained clustered at a single cell pole during the outgrowth of cells lacking McdA (Fig. 2E-F; Video S3). Upon McdA co-expression, encapsulins rapidly redistributed into multiple foci across the cell during outgrowth (Fig. 2G-H; Video S3). Reducing McdA levels caused distributed encapsulins to revert to polar clusters, confirming that positioning requires sustained McdA activity (Fig. 2I-J; Video S4). Conversely, adding McdA to cells with pre-aggregated encapsulins triggered their redistribution along the cell length (Fig. 2K-L; Video S4). Together, these results establish that McdA can spatially control MapTagged encapsulins, with its presence or absence dynamically switching organelles between dispersed and clustered states.

We further performed cryo-ET analysis to confirm that without McdA, the punctate foci represent fully assembled encapsulin clusters confined to the cell pole (Fig. 2M). By contrast, in McdA-expressing cells, encapsulins were no longer restricted to the poles. Instead, we observed encapsulins distributed along the nucleoid region of the cell (Fig. 2N), consistent with fluorescence imaging.

The results thus far demonstrate that the McdAB system from *H. neapolitanus* can be harnessed for minimal, autonomous spatial control of carboxysomes and encapsulins in *E. coli*. α-carboxysomes are both structurally and phylogenetically distinct from β-carboxysomes found in β-cyanobacteria. To extend the versatility of this system, we developed a complementary β-MapTag derived from the N-terminal region of McdB from the β-carboxysome positioning system of the β-cyanobacterium *Synechococcus elongatus*. Expressing β-MapTagged-encapsulins alongside *S. elongatus* McdA, also resulted in encapsulins being distributed across the *E. coli* nucleoid (Supplementary Fig. 2D-H). Together, these findings establish α- and β-MapTags as broadly applicable systems for programmable spatial control of engineered encapsulin nanocompartments.

Spatial control of biomolecular condensates

While BMCs and encapsulins have long been recognized as bacterial organelles, biomolecular condensates have only recently emerged as a distinct strategy for organizing cellular reactions in bacteria (*16*). Their dynamic and reversible nature makes condensates attractive for biotechnology (*17*), yet in bacteria, they typically coalesce into a single polar focus, causing asymmetric inheritance during division (*3*, *18*). To address this limitation, we engineered a condensate positioning system using

the MapTag.

S. elongatus McdB forms nucleoid-excluded condensates when expressed in *E. coli* (*18*). We first asked whether McdA could redistribute these condensates on the nucleoid. When expressed alone, mNG-McdA colocalized with the *E. coli* nucleoid (Supplementary Fig. 3A-B). Intriguingly, co-expression with McdB abolished this association. Because McdB condensates are highly fluid-like and a substantial fraction remains cytoplasmic (*18*), we hypothesized that this cytoplasmic McdB pool globally stimulates McdA release from the nucleoid. To reduce these spurious interactions away from the condensate cargo, we fused McdB to the PopTag (*19*), which enhanced McdB sequestration into condensates (Supplementary Fig. 3C-D). Without McdA, McdB^{PopTag} formed one or two large polar condensates (Fig. 3A, C-D). But upon McdA co-expression, multiple condensates were distributed along the nucleoid (Fig. 3B, C-D).

Without McdA positioning, polar condensates were rapidly lost from the cell population (Fig. 3E-F; Video S5). By contrast, in the presence of McdA, all daughter cells inherited roughly an equal complement of McdB^{PopTag} condensates distributed over the nucleoid (Fig. 3G-H; Video S5). Reducing McdA levels resulted in distributed condensates merging back into a single large nucleoid-excluded condensate at the cell pole (Fig. 3I-J; Video S6). Conversely, we observed that replenishing McdA led to the dissolution of polar condensates and the formation of multiple condensates distributed along the nucleoid (Fig. 3K, L; Video S6). Finally, we also confirmed the relocalization of polar condensates to the nucleoid in the presence of McdA by *in situ* cryo-ET (Fig. 3M-N). Our cryo-ET analysis revealed that the addition of tags and the repositioning system does not change the material properties of the condensate.

After successfully engineering a system that allowed us to distribute full-length β-McdB condensates, we set out to identify the minimal β-MapTag sequence for spatially regulating condensates with McdA. The first 20 N-terminal amino acids of β-McdB fused to mCherry^{PopTag} did not yield any condensates (Supplementary Fig. 4A-B). However, addition of the adjacent coiled-coil dimerization domain of β-McdB provided additional valency that restored condensate assembly (Supplementary Fig. 4C). Co-expression of McdA distributed these β-MapTagged condensates along the nucleoid (Supplementary Fig. 4D-F). When swapping the β-MapTag with the α-MapTag, co-expression with its cognate McdA resulted in condensate dissolution over the nucleoid (Supplementary Fig. 4G-I), suggesting the α-MapTag may be more suitable for positioning condensates with lower saturation concentrations. Together, we demonstrate that McdA can direct the spatial organization of both McdB condensates and MapTagged condensates, ensuring their cellular distribution and faithful inheritance across the cell population.

Spatial control of a membrane-bound organelle

To test the versatility and robustness of MapTags, we determined if this mode of spatial control could be extended beyond protein-based compartments to include membrane-

bound organelles. Ferrosomes are membrane-bound compartments for iron storage that require the membrane protein FezA and the P1B6-ATPase transporter FezB for their formation (*20*). Heterologous expression of FezA and FezB in *E. coli* induces the formation of these lipid-bound compartments. Expression of mNG-FezB fused to the α-MapTag, along with untagged FezA, resulted in the formation of ferrosome clusters at the cell pole (Fig. 4A, C-D; Supplementary Fig. 5A-B). Upon co-expression of McdA, multiple ferrosome foci were observed over the nucleoid (Fig. 4B, C-D; Supplementary Fig. 5A-B). A co-expression time course showed McdA ensuring the cellular distribution and faithful inheritance of assembling ferrosomes across the cell population (Fig. 4E-F). We observed that McdA was also able to partition preformed ferrosome clusters at the cell pole and redistribute them over the nucleoid (Fig. 4G-H). Finally, we observed that using the β-MapTag to FezB was just as effective in distributing ferrosomes as the α-MapTag (Supplementary Fig. 5C-D).

Discussion

We establish spatial control as a new design principle in bacterial synthetic biology. By reconstituting and repurposing McdAB, we show that a minimal, two-protein positioning module can be harnessed to restore the native organization of carboxysomes and, more broadly, to spatially reprogram the distribution of diverse bacterial organelles in *E. coli*. The capacity to engineer both the composition of cellular compartments and their precise intracellular positioning advances synthetic biology into a new era, where the spatial context of cellular function ("where") can be programmed as readily as its molecular content ("what").

The impact of this spatial control extends beyond simple organelle placement. We demonstrate that mislocalized carboxysomes in *E. coli* also suffer structural defects. McdAB corrects this by transforming disordered polar aggregates into properly sized and structurally intact organelles distributed over the nucleoid, restoring both assembly fidelity and inheritance. By generalizing this approach with MapTags, we extend spatial control to encapsulins, condensates, and ferrosomes - representing the full spectrum of known protein-based and lipid-bound organelle types. These results suggest that spatial misregulation may be a universal bottleneck for heterologous organelle engineering, and that positioning systems provide a general solution.

This conceptual advance parallels the way cytoskeletal elements and trafficking systems underpin compartmentalization in eukaryotes. Whereas eukaryotes evolved complex, multi-component transport machinery, bacteria have distilled spatial organization into minimal ATP-driven modules that establish self-organizing gradients. By reengineering this strategy, we unlock a scalable, orthogonal method for positioning organelles in bacterial cells. The versatility of α- and β-MapTags across structurally distinct compartments underscores their potential as modular "address labels" for intracellular engineering.

Programmable organelle positioning opens several future directions. First, it enables the rational design of metabolic “reaction landscapes” in bacteria, where organelles can be spaced to prevent interference, aligned to channel substrates, or dynamically repositioned in response to environmental signals. Second, because McdAB activity is reversible, spatial organization can be toggled on or off, allowing for time-dependent control of metabolism or stress responses. Third, distributing compartments evenly across the nucleoid ensures faithful inheritance, reducing population-level heterogeneity and thereby improving the reliability of engineered microbial systems. By layering spatial control onto existing advances in compartment design, we foresee the emergence of “organelle engineering” as a discipline in its own right - where the content, function, and location of organelles can all be rationally specified. Such a framework could accelerate the development of microbial cell factories for carbon capture, green chemistry, and therapeutics.

Beyond biotechnology, this work provides a blueprint for constructing synthetic cells. A central question in bottom-up biology is how to couple self-assembly with inheritance. Our results demonstrate that a minimal gradient-based system is sufficient to transform self-assembling but static compartments into dynamic, heritable organelles.

Acknowledgements

We thank Dr. Eric Rentchler and Dr. Sasha Meshinchi of the Biomedical Microscopy Core at the University of Michigan for training and coordinating access to the super-resolution Airyscan Microscope. A provisional patent application related to this work (PCT/US24/50743) has been filed.

Funding:

National Science Foundation grant 1941966 (A.G.V)

National Institutes of Health grant R35GM152128 (A.G.V.)

National Institutes of Health 1K99GM157383-01 (Y.H.)

National Institutes of Health 1DP2GM150019-01 (S.M.)

Klatskin Sutker Discovery Fund (S.M.)

National Institutes of Health grant S10OD030275 (S.M.)

Arnold and Mabel Beckman Foundation award to the University of Michigan Cryo-EM facility

National Institutes of Health T32 GM145304 (J.A.B.)

The funders had no role in the study design, data collection, analysis, or the content and publication of this manuscript.

Author contributions:

Conceptualization: A.G.V. and Y.H.

Methodology: A.G.V., Y.H., P.V.J., D.S.T., R.E.D., S.K., K.T., J.A.B., C.A.A., T.W.G., H.P., and S.M.

Investigation: A.G.V., Y.H., P.V.J., S.M.

Visualization: A.G.V., Y.H., R.E.D., J.A.B.

Funding acquisition: A.G.V., Y.H., S.M., T.W.S., H.P.

Project administration: A.G.V. and Y.H.

Supervision: A.G.V. and S.M.

Writing – original draft: A.G.V. and Y.H.

Writing – review & editing: All authors

Competing interests:

The authors declare that they have no competing interests.

Data and materials availability

All plasmids are available at Addgene. Data processing and analysis scripts for this study are available on GitHub.

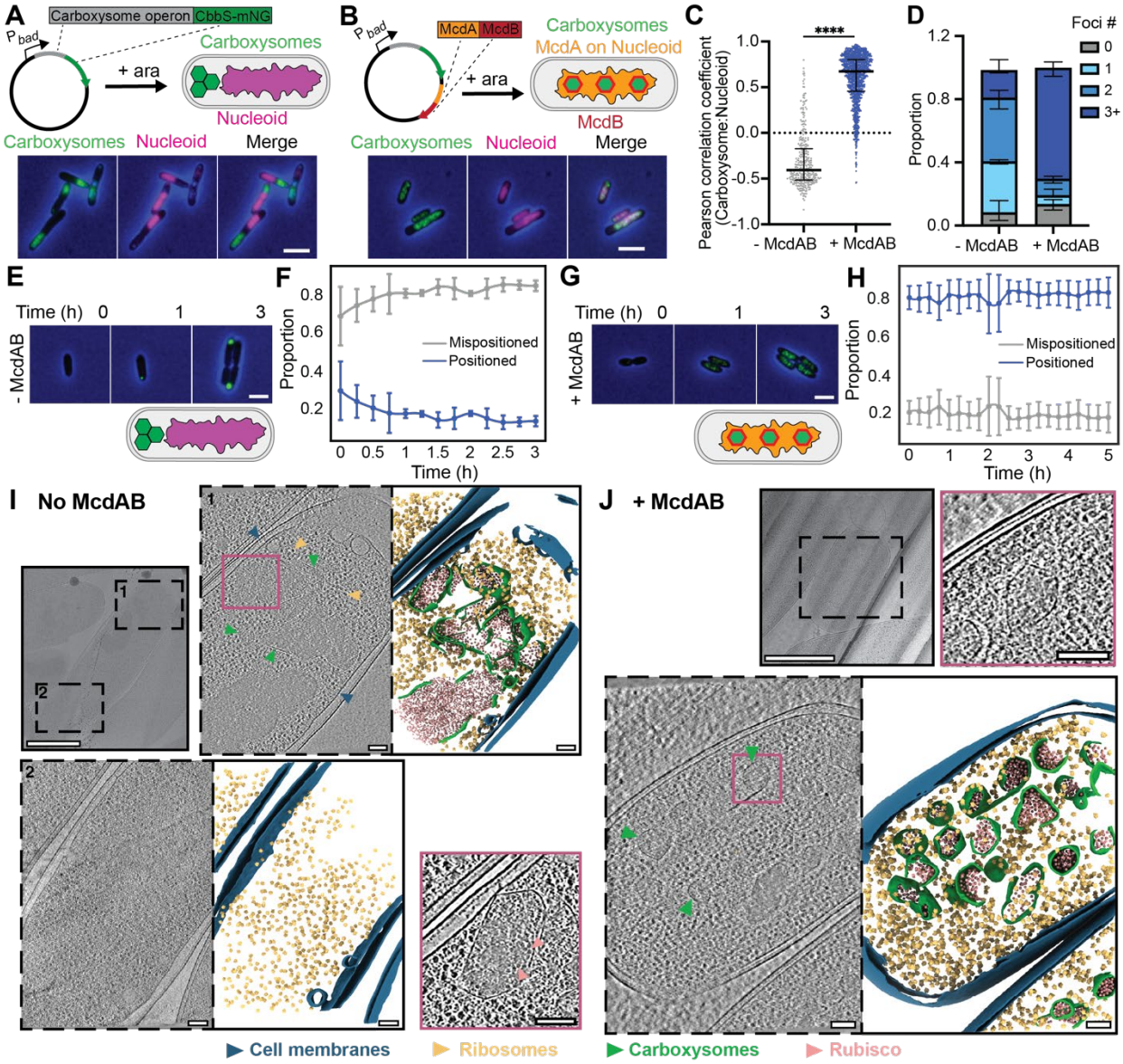

Figure 1. The McdAB system spatially organizes carboxysomes on the *E. coli* nucleoid. (**A**, **B**) Schematic and wide-field fluorescence images of *E. coli* cells expressing carboxysomes without (A) or with (B) the McdAB system. The small subunit of Rubisco (CbbS) is fused to mNeonGreen (mNG); protein expression is induced with 0.2% arabinose (ara). Unless specified, mNG-labeled carboxysomes are shown in green, DAPI-stained nucleoids in magenta, and phase-contrast in blue; scale bar, 2 µm. (**C**) Pearson correlation coefficients measuring colocalization between mNG-carboxysomes and DAPI-stained nucleoids. (**D**) Quantification of the proportion of cells with indicated numbers of carboxysome foci. (**E**–**H**) Time-lapse analysis showing images and quantification of carboxysome positioning over time with (E, F) or without (G, H) McdAB. Proportions of cells with mispositioned (0–2 polar foci) and positioned (≥ 3 distributed foci) carboxysomes are plotted over time. (**I, J**) Cryo-electron tomography of *E. coli* without (I) or with (J) the McdAB system. In each case, low-magnification (6500×) transmission electron microscopy (TEM) images are shown to the left and indicate sites of tomography tilt series data acquisition (dashed boxes). Representative slices through tomograms (dashed boxes) and corresponding segmentations of the tomograms are shown in each case. Cellular

features are highlighted as carboxysomes (green), Rubisco (pink), ribosomes (orange), and cell membranes (blue). Zoomed-in views (pink boxes) provide higher-magnification images of carboxysomes (with Rubsico marked with pink arrowheads). Scale bars: 500 nm (overview), 100 nm (zoom-in).

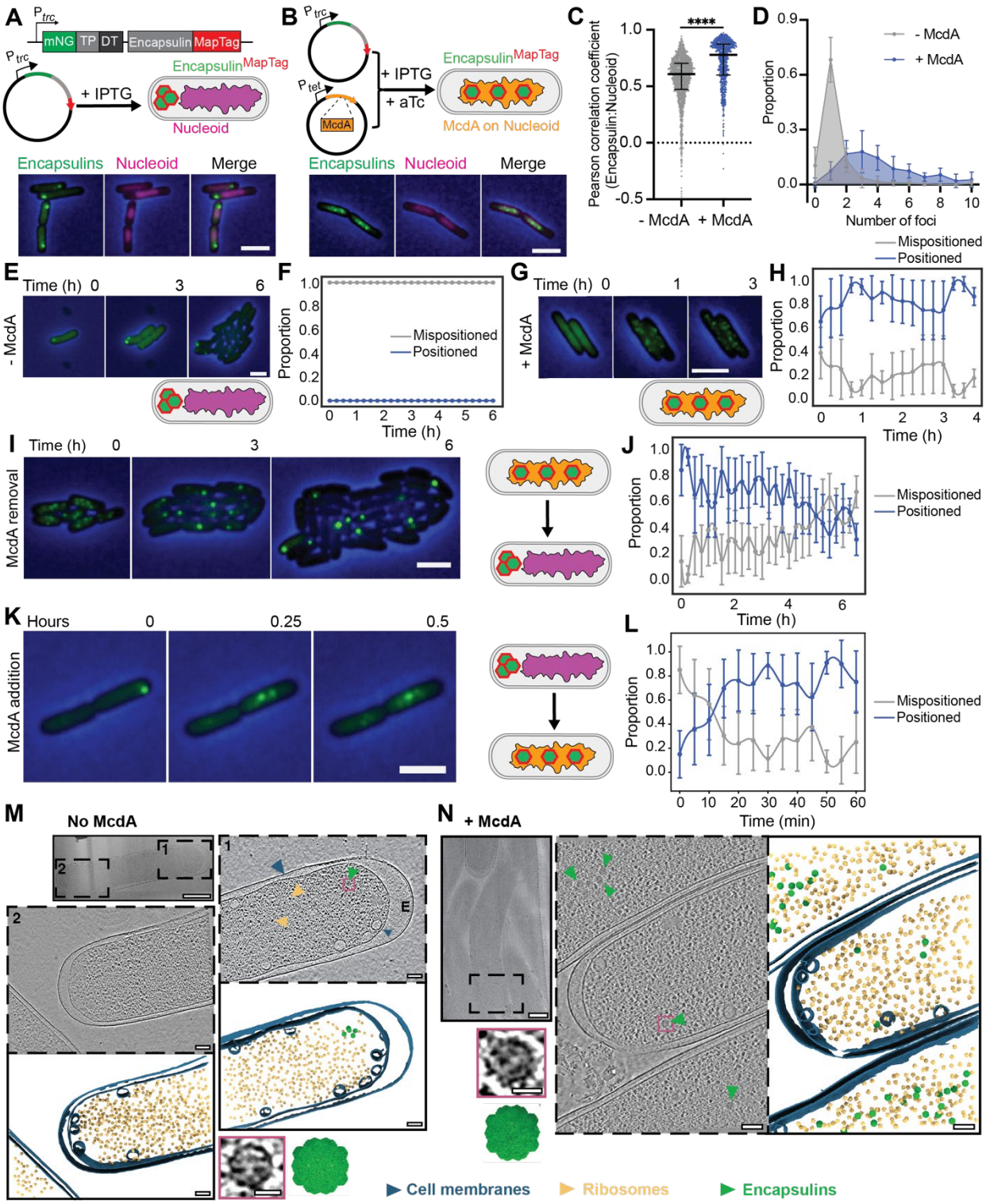

Figure 2. McdA distributes MapTagged encapsulins on the *E. coli* nucleoid. (**A**) Schematic and wide-field fluorescence images of *E. coli* cells expressing encapsulins fused to the MapTag and mNeonGreen (mNG) cargo fused to an encapsulin-specific targeting peptide (TP) and a degron tag (DT), under the P_{trc} promoter with IPTG induction. (**B**) As in (A), but with McdA co-expressed from a separate plasmid under the P_{tet} promoter, induced with anhydrotetracycline (aTc). Unless specified, mNG-labeled encapsulins are shown in green, DAPI-stained nucleoids

in magenta, and phase-contrast in blue; scale bars, 2 µm. (**C**) Pearson correlation coefficients measuring colocalization between mNG-encapsulins and DAPI-stained nucleoids. (**D**) Quantification of the proportion of cells with the indicated number of encapsulin foci. (**E**–**H**) Time-lapse analysis showing images and quantification of encapsulin positioning over time in cells without (E, F) or with (G, H) McdA; proportions of cells with mispositioned (0–2 polar foci) and positioned (≥3 distributed foci) encapsulins are shown. (**I**–**L**) Reversible control of encapsulin positioning through McdA removal (I, J) or addition (K, L), as shown by images and quantification of positioned and mispositioned encapsulins over time. (**M**, **N**) Cryo-electron tomography of encapsulin^{MapTag}-containing *E. coli* without (M) or with (N) McdA. In each case, low-magnification (6500×) transmission electron microscopy (TEM) images are shown to the left and indicate sites of tomography tilt series data acquisition (dashed boxes). Representative slices through tomograms (dashed boxes) and corresponding segmentations of the tomograms are shown in each case. Cellular features are highlighted as encapsulins (green), ribosomes (orange), and cell membranes (blue). Zoomed-in views (pink boxes) provide higher-magnification images of fully assembled encapsulins. Scale bars: 500 nm (overview), 100 nm (zoom-in).

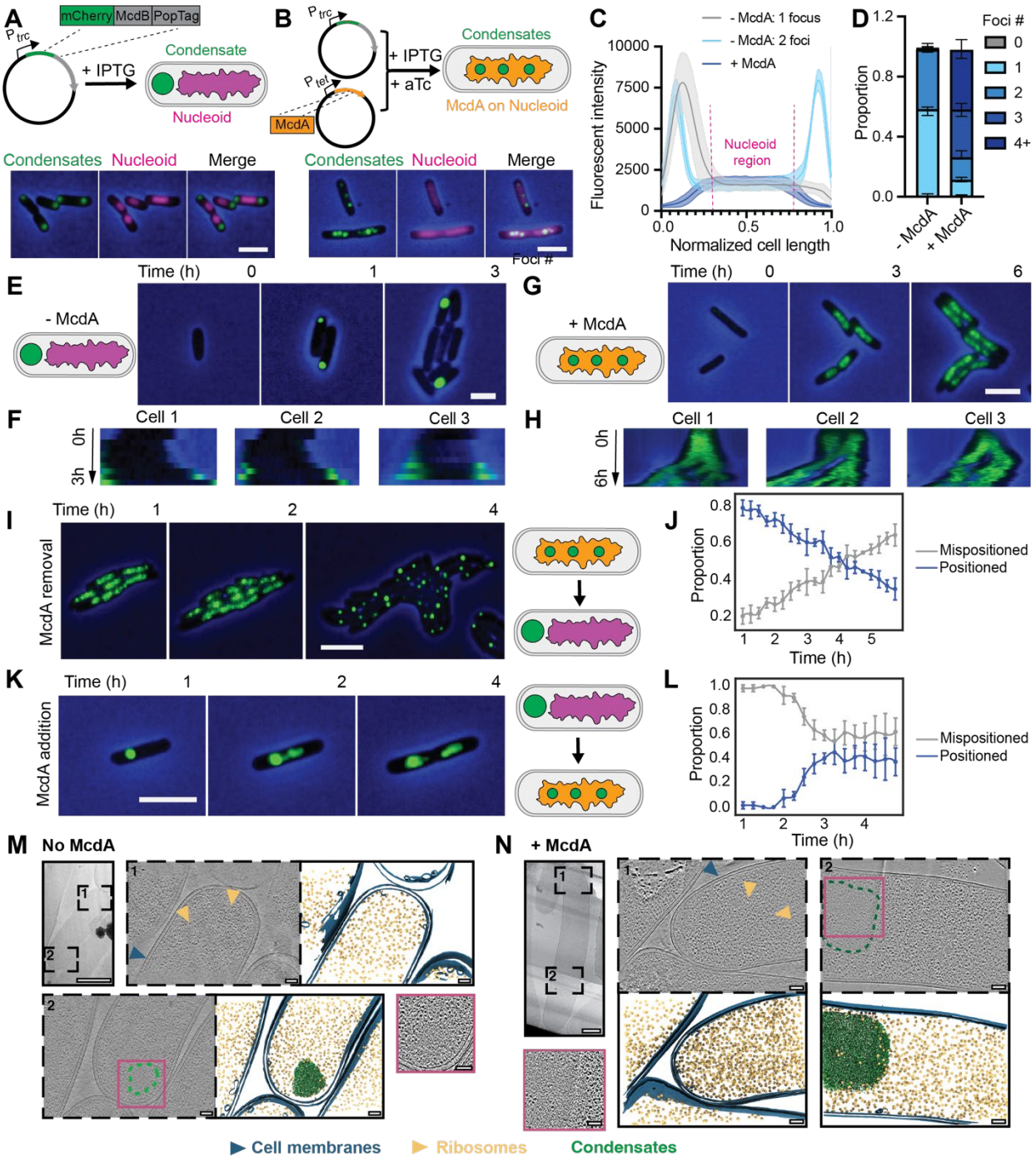

Figure 3. McdA distributes McdB condensates on the *E. coli* nucleoid. (**A**) Schematic and wide-field fluorescence images of *E. coli* cells expressing McdB condensates fused to mCherry and PopTag, under the P_{trc} promoter with IPTG induction. (**B**) As in (A), but with McdA co-expressed from a separate plasmid under the P_{tet} promoter, induced with anhydrotetracycline (aTc). Unless specified, $McdB^{PopTag}$ condensates are shown in green, DAPI-stained nucleoids in magenta, and phase-contrast in blue; scale bars, 2 µm. (**C**) Fluorescent intensity profiles of $McdB^{PopTag}$ signal along the normalized cell length. (**D**) Quantification of the proportion of cells with the indicated number of $McdB^{PopTag}$ condensates. (**E–H**) Time-lapse analysis showing wide-field fluorescence images (E, G) and kymographs of representative cells (F, H) depicting the

distribution of McdB^{PopTag} fluorescence over time without (E, F) or with (G, H) of McdA. (**I–L**) Reversible control of McdB^{PopTag} condensate positioning by McdA removal (I, J) or addition (K, L), shown by wide-field fluorescence images and quantification of positioned(≥3 distributed foci) and mispositioned (0–2 polar foci) condensates over time. (**M**, **N**) Cryo-electron tomography of *E. coli* expressing McdB^{PopTag} condensates without (M) or with (N) McdA. In each case, low-magnification (6500×) transmission electron microscopy (TEM) images are shown to the left and indicate sites of tomography tilt series data acquisition (dashed boxes). Representative slices through tomograms (dashed boxes) and corresponding segmentations of the tomograms are shown in each case. Cellular features are highlighted as condensates (green), ribosomes (orange), and cell membranes (blue). Zoomed-in views (pink boxes) provide higher-magnification images of condensates seen as ribosome-excluded areas. Scale bars: 500 nm (overview), 100 nm (zoom-in).

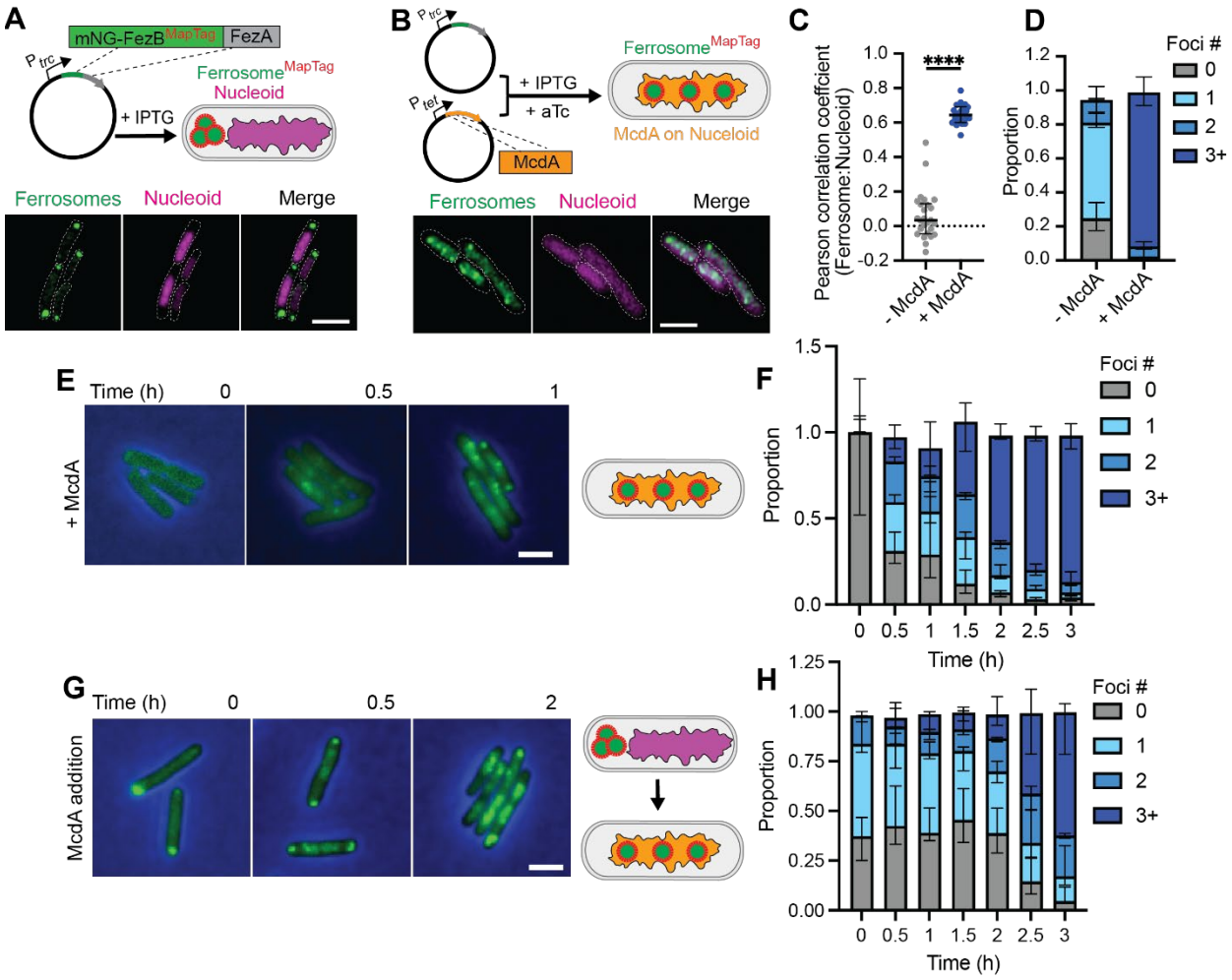

Figure 4. McdA distributes MapTagged ferrosomes on the *E. coli* nucleoid. (**A**) Schematic and super-resolution Airyscan images of *E. coli* cells expressing ferrosomes, composed of FezA and FezB (with FezB fused to mNeonGreen [mNG]), under the P_{trc} promoter with IPTG induction. (**B**) As in (A), but with McdA co-expressed from a separate plasmid under the P_{tet} promoter, induced with anhydrotetracycline (aTc). Unless specified, ferrosomes are shown in green, DAPI-stained nucleoids in magenta, and phase-contrast in blue. Scale bars, 2 µm. (**C**) Pearson correlation coefficients measuring colocalization between mNG-labeled ferrosomes and DAPI-stained nucleoids. (**D**) Quantification of the proportion of cells with the indicated number of ferrosome foci. (**E**, **F**) Wide-field fluorescence images (E) and quantification (F) of ferrosome positioning over time in cells with McdA over time. (**G**, **H**) Wide-field fluorescence images (G) and quantification (H) showing the redistribution of ferrosomes upon McdA addition to cells initially lacking McdA over time.

Supplementary Information for:

Engineering Spatial Control of Bacterial Organelles

Y Hoang[†], Pankaj. V. Jadhav[†], Daniel S. Trettel, Rachel E. Dow, Seokmu Kwon, Kate Matej, Jordan A. Byrne, Christopher A. Azaldegui, Tobias W. Giessen, Hualiang Pi, Shyamal Mosalaganti[*], and Anthony G. Vecchiarelli*

[†] These authors contributed equally

* Correspondence: ave@umich.edu (A.G.V.), mosalaga@umich.edu (S.M.)

This file includes:

Materials and Methods

Supplementary Figures S1-S5

Supplementary Tables 1-5

Description of Video Files

References

Materials and Methods

Plasmid construction

Primers, plasmids, and strains used in this study can be found in Supplementary Tables 1 & 2. Plasmids were cloned using Gibson assembly and transformed into competent *E. coli* DH5α cells, transformants selected on LB plates supplemented with the corresponding antibiotics.

Carboxysomes**:** Plasmids encoding fluorescently tagged CbbS with McdAB were generated using Gibson assembly. For example, to create pDT081, the previously published carboxysome-only construct pDT074 (*4*) was PCR-linearized with Q5 polymerase and primers oDT077/oDT098 (15 s/kb extension, 65°C annealing, 27 cycles). The 13.7 kb amplicon was treated with DpnI (37°C, 30 min), purified (Zymo PCR Clean and Concentrator Kit), and eluted in deionized water. The *H. neapolitanus* McdAB cassette (gDT062; Twist Biosciences), codon-optimized for *E. coli* and containing each gene preceded by the strong BBa_0030 ribosome binding site, was assembled with 0.020 pmol linearized vector and 0.060 pmol gDT062 using the NEBuilder HiFi DNA Assembly kit (50°C, 20 min). Gibson reactions were immediately frozen at −20°C and transformed into NEB5alpha competent cells by heat shock. Colony screening was performed by whole-plasmid sequencing (Plasmidsaurus). Plasmids pDT082 and pDT084 were constructed from the published plasmids pDT075 and pDT078 using a similar strategy.

Encapsulins**:** Plasmid pSMK1, for the expression of encapsulin fused to mNeonGreen and an α-MapTag, was generated by Gibson assembly of a pTrc99A backbone (*18*) with a synthetic, *E. coli* codon-optimized gene fragment encoding mNeonGreen and α-McdB-tagged encapsulin. Plasmid pSMK2 was prepared by replacing the α-McdB tag in pSMK1 with a β-MapTag, using overhang PCR with primers pSMK23-F and pSMK2-R. Plasmid pYH84, used to express McdA from *H. neapolitanus*, was constructed by Gibson assembly of a pBbA2k backbone (*21*) with a synthetic, *E. coli* codon-optimized gene fragment encoding *H. neapolitanus* McdA. Plasmid pYH91, for expression of McdA from *S. elongatus*, was generated using the same strategy with a corresponding gene fragment.

Condensates**:** Plasmid pYH82, which expresses the McdB^{PopTag} condensate, was constructed by Gibson assembly. The backbone was amplified from pYH77 (*18*) using primers YH20 and YH21, and the *S. elongatus* McdB fragment was amplified from pYH71 using primers YH22 and YH23. The plasmid pJAB30 was constructed by amplifying pYH82 with primers YH24 and YH25, followed by ligation with KLD Enzyme Mix (New England Biolabs), transformation into *E. coli* DH5α, and plasmid verification by Plasmidsaurus. The plasmid pJAB39 was generated using a similar strategy with primers YH26 and YH27.

Ferrosomes**:** To construct pKM1, pSMK1 was sequentially digested with NcoI-HF and SalI-HF at 37°C for one hour per enzyme, and the plasmid backbone was purified using a gel extraction kit. A GeneBlock containing α-MapTag-mNeonGreen was obtained from Integrated DNA Technologies and amplified with primers KM1/KM2. FezA and FezB were amplified from *C. difficile* CD196 genomic DNA using the primers KM3/KM4 and KM5/KM6, respectively. PCR products were purified (Qiagen PCR purification kit) and assembled with the backbone in a four-piece HiFi DNA Assembly reaction, then transformed into *E. coli* DH5α. Resulting plasmids were mini-prepped and verified by whole-plasmid sequencing (Plasmidsaurus). For construction of pKM2, a GeneFragment encoding the β-MapTag sequence was obtained from Genewiz. pKM1

and the GeneFragment were digested with KasI and BamHI-HF at 37°C for one hour, then purified via gel extraction. The fragments were ligated with T4 DNA ligase at room temperature for 16 hours and transformed into *E. coli* DH5α. Plasmids were mini-prepped and correct insertion was verified by Sanger sequencing (Keck DNA Sequencing Facility, Yale University).

Media and culture growth

For routine bacterial growth, LB medium was used for all overnight cultures. Single colonies were inoculated into 15 mL Falcon tubes containing LB broth and grown overnight at 37°C with agitation (200-225 rpm) for 12-16 hours. Exponential phase cultures were initiated by diluting overnight cultures 1:100 into LB or AB minimal medium. Carboxysome expression experiments in *E. coli* Top10 were performed in LB medium, while protein induction experiments in *E. coli* MG1665 were carried out in AB minimal medium. AB medium was supplemented with 0.2% carbon source (glycerol for growth or glucose to minimize basal expression from the P_{trc} promoter), 0.2% casamino acids, 10 µg/mL thiamine, and 25 µg/mL uracil (*22*). Where appropriate, antibiotics were added at the following final concentrations: carbenicillin (100 µg/mL), kanamycin (100 µg/mL), and chloramphenicol (100 µg/mL). Protein induction was achieved using IPTG, anhydrotetracycline (aTc), or arabinose at concentrations detailed in each experiment. Strains and plasmids are listed in Table S1. Reagents are listed in Supplementary Table 3.

Expression of organelles

Carboxysomes: *E. coli* Top10 cells were transformed with plasmid pDT074 to express mNeonGreen-labeled carboxysomes. For respective carboxysomes with the McdAB system, pDT81 was used. Overnight cultures were diluted and grown in LB medium until an optical density (OD_{600}) of 0.2–0.6 was reached. Carboxysome expression was induced with 0.2% arabinose for 2 hours. For fluorescently labeled variants, pDT075 and pDT082 were used for mScarlet-labeled carboxysomes, and pDT078 and pDT084 for mJuniper-labeled carboxysomes.

Encapsulins: *E. coli* MG1655 *ΔlacY* cells were transformed with plasmid pSMK1 to express encapsulin$^{\alpha\text{-MapTag}}$. Exponential phase cultures in AB media were induced with 1 mM IPTG for 2 hours. For co-expression of McdA, cells were co-transformed with pSMK1 and pYH84 and induced with 1 mM IPTG and 20 nM aTc. For encapsulin$^{\beta\text{-MapTag}}$, plasmids pSMK2 and pYH91 were used under similar induction conditions.

Biomolecular condensates**:** For full-length McdB^{PopTag} condensates, *E. coli* MG1655 *ΔlacY* cells were transformed with plasmid pYH82. Exponential phase cultures in AB medium were induced with 100 µM IPTG for 2 hours. For co-expression with McdA, cells were co-transformed with pYH82 and pYH91 and induced with 100 µM IPTG and 5 nM aTc. For α- and β-MapTag-tagged condensates, cells were co-transformed with pJAB39 and pYH82, or with pRED2 and pYH84, respectively, and induced under the same conditions.

Ferrosomes**:** For ferrosome$^{\alpha\text{-MapTag}}$, *E. coli* MG1655 *ΔlacY* cells were transformed with plasmid pKM1. Exponential phase cultures in AB medium were induced with 1 mM IPTG for 2 hours. For co-expression with McdA, cells were co-transformed with pKM1 and pYH84 and induced with 1 mM IPTG and 20 nM aTc. For ferrosome$^{\beta\text{-MapTag}}$, cells were co-transformed with pKM2 and pYH91 and induced under the same conditions.

McdA removal and addition assays

To reduce McdA protein levels in cells with positioned organelles, cultures were washed (5,000 rpm for 2 minutes, three times) and resuspended in fresh medium containing IPTG but lacking aTc, the inducer for McdA. As cells grew and divided, McdA levels decreased by generational dilution. Cells were monitored by live-cell imaging. In a complementary experiment, cells containing both organelle and McdA plasmids were initially induced with IPTG (1 mM) in the absence of aTc, resulting in aggregated, polar-localized compartments. Upon addition of aTc (20 nM) to these cultures, time-lapse imaging was performed to monitor compartment redistribution.

DAPI staining and chloramphenicol treatment

DAPI was added to exponentially growing cultures at a final concentration of 2 μM and incubated for 15 min at 37°C before imaging, without rinsing. DAPI fluorescence was detected using the “DAPI” filter set as described in the “Wide-field fluorescence and phase-contrast imaging” section. For nucleoid compaction, chloramphenicol was added to exponentially growing cultures at a final concentration of 100 μg/mL, followed by incubation at 37°C for 30 min before imaging.

Wide-field fluorescence and phase-contrast imaging

Wide-field fluorescence and phase-contrast imaging were performed using a Nikon Ti2-E motorized inverted microscope controlled by the NIS Elements software with a SOLA 365 LED light source, a 100 × objective lens (Oil CFI Plan Apochromat DM Lambda Series for Phase Contrast), and a Photometrics Prime 95B back-illuminated sCMOS camera or Hamamatsu Orca-Flash 4.0 LTS camera. Fusions to mNeonGreen and mJuniper were imaged using a “GFP” filter set (C-FL GFP, Hard Coat, High Signal-to-Noise, Zero Shift, Excitation: 436 ± 10 nm, Emission: 480 ± 20 nm, Dichroic Mirror: 455 nm). DAPI fluorescence was imaged using a “DAPI” filter set (C-FL DAPI, Hard Coat, High Signal-to-Noise, Zero Shift, Excitation: 350 ± 25 nm, Emission: 460 ± 25 nm, Dichroic Mirror: 400 nm). mScarlet and mCherry was imaged using a “Texas Red” filter set (C-FL Texas Red, Hard Coat, High Signal-to-Noise, Zero Shift, Excitation: 560 ± 20 nm, Emission: 630 ± 37.5 nm; Dichroic Mirror: 585 nm).

Time-lapse videos of protein induction

To visualize the dynamics of organelle positioning, exponential-phase cultures were induced with either IPTG alone or with both IPTG and aTc. A 2 μL aliquot of culture was then spotted onto agarose pads (LB medium for carboxysomes; AB medium for encapsulins and condensates) in 35-mm glass-bottom dishes, with cells positioned between the agar pad and the glass surface. Time-lapse images were captured using the phase contrast and “GFP” filter set (see "Wide-field fluorescence and phase-contrast imaging" section) every 15 min for 3 hours. For McdA removal experiments, cultures were washed, resuspended in fresh medium lacking aTc, and spotted onto AB agarose pads without aTc. For McdA addition experiments, cultures 2 hours post-IPTG induction were spotted onto AB agarose pads containing 20 nM aTc.

Super-resolution imaging

Cells were spotted onto agar pads in glass-bottom dishes for imaging. Super-resolution images were acquired using a Zeiss LSM 980 Airyscan 2 microscope equipped with a 63×/1.4 NA Plan

Apo oil objective (190 µm working distance). mNeonGreen fluorescence was excited with a 488 nm laser and detected with the Airyscan 2 detector. Images were post-processed using Zen 3.4 (Blue edition).

Cryo-electron tomography (cryo-ET) of *E. coli*

Sample vitrification**:** Bacterial samples were first concentrated to an OD_{600} of ~40 by centrifugation at 500 × g for 5 min. Subsequently, 3 µL of the concentrated bacterial cell suspension was applied to glow-discharged R1/4, 200 mesh holey copper grids (Quantifoil Micro Tools GmbH). Grids were single-side blotted for 5 s with a blot force of 10 at 30 °C and 95% humidity before being plunge-frozen in liquid ethane using Vitrobot Mark IV (ThermoFisher Scientific), clipped onto AutoGrids (ThermoFisher Scientific), and stored in liquid N_2 till further use.

Cryo-focused ion beam milling (cryo-FIB) and tilt series acquisition**:** Clipped grids were loaded onto an Aquilos 2 dual-beam microscope (Thermo Fisher Scientific), maintained at ≤−190 °C. Grids were coated with a layer of organometallic platinum using a gas injection system (GIS) for 30 s and subsequently sputter-coated for 20s. The lamella milling sites were selected using the MAPS 3.25 software (Thermo Fisher Scientific). At each site chosen, tension-relief trenches were milled with a beam current of 1 nA. Subsequently, ~5 µm-thick lamellae were milled at an angle of 6 degrees. Following this, lamellae were thinned stepwise to ~1 µm thickness with beam currents of 500–100 pA. Finally, all lamellae were polished to a final thickness of ~200 nm with a beam current of 50 pA. Tilt series were acquired on a Titan Krios G4i transmission electron microscope (Thermo Fisher Scientific) operated at 300 kV, equipped with a K3 direct-electron detector (Gatan Inc.) and a Bioquantum energy filter (Gatan Inc.). Montages of lamella were collected at a magnification of 6500× to identify cells with features of interest. Movies were collected at a magnification of 33,000× in super-resolution mode and binned 2×, corresponding to a nominal physical pixel size of 2.654 Å, with 9 frames per tilt. Tilts series were collected using SerialEM software v4.1 (PMID: 16182563) with a dose-symmetric tilt scheme (PMID: 32054835) with 3° tilt increment from -60 ° to +60°, starting from a + 6° pretilt. The total dose per tilt series was 120 $e^-/Å^2$.

Tilt series pre-processing, alignment, and tomogram reconstruction**:** Motion correction and contrast transfer function (CTF) estimation were performed using WarpTools v2.0.0 (*23*). Subsequently, motion-corrected tilts were aligned using patch tracking in batch mode using a custom bash script and, if required, optimized manually in IMOD v4.11.25 (PMID: 27444392). The resulting alignment files were imported into Warp. 4× binned tomograms, resulting in a pixel size of 10.60 Å, were reconstructed using WarpTools and used for downstream analysis.

Membrane tracing and voxel segmentation**:** The binned tomograms were processed by Membrain-Seg (*24*) for tracing and segmenting cellular membranes and carboxysomes. The traced volumes were imported into AMIRA (Thermo Fisher Scientific) for manual curation. Next, smooth surfaces were generated from the membrane and carboxysome labels. These surfaces were imported into ChimeraX (PMID: 37774136) for final rendering. Template matching was performed using WarpTools to segment ribosomes using the *E. coli* 70S ribosome density map (EMD-13270) (PMID: 35022621) as the template. The resulting particle picks were manually curated to get the final ribosome particle coordinates. These coordinates were used to place ribosomes in ChimeraX using the AtriaX v0.6.0 plugin (PMID: 36251681). Rubisco and

encapsulins were manually picked in the tomograms, and the particle coordinates were imported into ChimeraX to place the Rubisco (EMD-15409) (PMID: 37015227) and encapsulin (EMD-5917) (PMID: 25024436) density maps into the volumes.

Image analysis

Cell segmentation**:** Cell segmentation was performed using the Omnipose package in Python as previously (*18*). For segmentation, a Gaussian blur (σ = 0.066 µm) was applied to phase-contrast images prior to processing with a custom-trained model (*18*). Cells touching the image borders were excluded. Erroneous segmentations were manually corrected with the Omnipose GUI or omitted from analysis.

Focus count analysis**:** Images from multiple fields of view were acquired as described above and analyzed using a custom Python script for fluorescent focus detection and analysis (*18*). Incorrectly identified fluorescent foci were manually filtered from further analysis. Detection parameters were optimized for each compartment type (see Supplementary Table 5). The number of cells with 0, 1, 2, or ≥3 foci was quantified and visualized using GraphPad Prism (GraphPad Software, San Diego, CA).

Fluorescence intensity profile analysis**:** Fluorescence intensity profiles were generated using ImageJ (Schneider et al. 2012). For each cell, a straight line was drawn across the longitudinal axis. The fluorescence intensity along the line was recorded. Cell length was normalized by rescaling the profile coordinates from 0 to 1. Cells without McdA were grouped and analyzed separately based on the number of observed foci (1 or 2). Cells expressing McdA were analyzed and plotted as a separate group. Intensity profiles were visualized using GraphPad Prism (GraphPad Software, San Diego, CA).

Kymograph analysis**:** Drift-corrected time-lapse image stacks were analyzed to generate kymographs representing fluorescence dynamics along the cell length. In Fiji (ImageJ) (Schneider et al. 2012), a straight line was manually drawn along the long axis of each cell. The Multi-Kymograph tool was used to extract intensity profiles. For visualization, intensity values at each time point were normalized to the minimum and maximum intensity within that frame. The resulting kymographs display the temporal evolution of fluorescence distribution along the cell axis.

Statistical Analysis

The experimental design, sample sizes, number of biological replicates, and statistical tests are summarized in Supplementary Table 4. In summary, distributions are presented as scattered plots, thick bar indicate the interquartile range around the median, and error bars represent a interquartile range. For XY graphs, shaded areas indicate the 95% CI. When applicable, P-values and statistical significance were evaluated using Kolmogorov-Smirnov (for distributions with at least 50 data points that do not assume normality) or One-Way ANOVA (for comparisons between two groups, with three data points each).

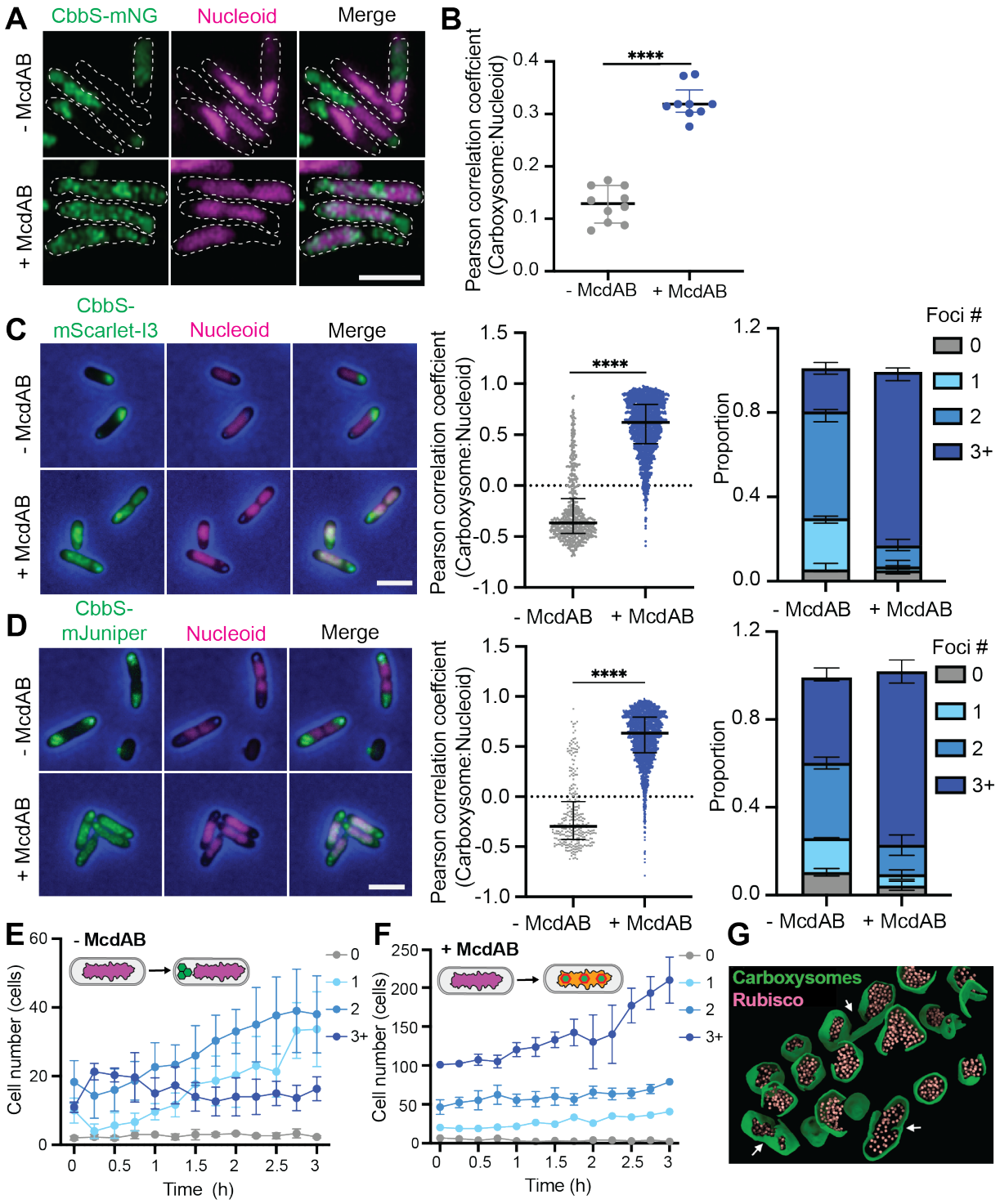

Supplementary Figure 1. The McdAB system spatially organizes carboxysomes on the *E. coli* nucleoid. (**A**) Super-resolution Airyscan images of cells without (top) or with (bottom) the McdAB system, showing mNeonGreen-labeled carboxysomes (green), DAPI-stained nucleoids (magenta); merged images are shown at right. Dashed outlines indicate cell boundaries. Scale bar, 2 µm. (**B**) Pearson correlation coefficients measuring colocalization between mNeonGreen-labeled carboxysomes and DAPI-stained nucleoids from cells in (A). (**C**, **D**) Wide-field fluorescence images of cells expressing carboxysomes labeled with mScarlet-I3 (C) or

mJuniper (D). Carboxysomes are shown in green, DAPI-stained nucleoids in magenta, and phase-contrast in blue; scale bar, 2 μm. Pearson correlation coefficients quantifying colocalization between labeled carboxysomes and DAPI-stained nucleoids, as well as the proportion of cells with 0, 1, 2, or ≥3 carboxysome foci, are provided. (**E**, **F**) Quantification of cells with 0, 1, 2, or ≥3 carboxysome foci without (E) or with (F) the McdAB system, corresponding to the cells in Fig. 1A-B. (**G**) Zoomed-in view of a segmented tomogram showing carboxysome partitioning in *E. coli* expressing the McdAB system (same as Fig. 1J). The arrows mark the invaginations or partitions in the carboxysome shells.

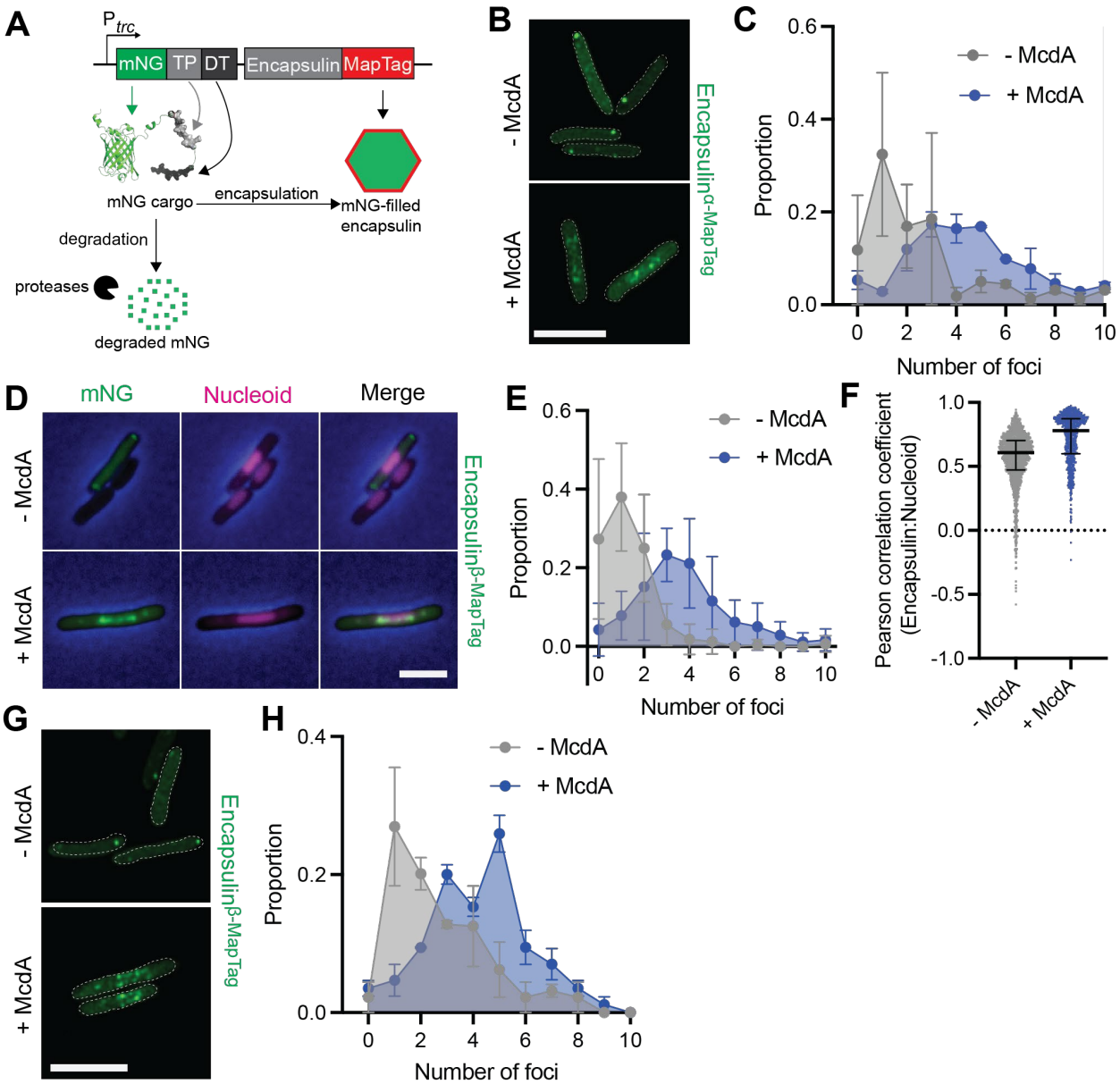

Supplementary Figure 2. McdA spatially organizes both α- and β-MapTagged encapsulins on the *E. coli* nucleoid. (**A**) Schematic illustrating the visualization strategy for encapsulins. The cargo protein mNeonGreen (mNG) is fused to an encapsuling-specific targeting peptide (TP) and a degron tag (DT), while the encapsulin monomer is fused to the MapTag. Unencapsulated mNG is targeted for degradation by cellular proteases, thereby enhancing the contrast for visualization of mNG-filled encapsulins. (**B**) Super-resolution Airyscan images showing encapsulin$^{\alpha\text{-MapTag}}$ (green) in cells without (top) or with (bottom) McdA. Scale bars, 2 µm. (**C**) Proportion of cells with the indicated number of encapsulin$^{\alpha\text{-MapTag}}$ foci from (B). (**D**) Wide-field fluorescence images showing encapsulin$^{\beta\text{-MapTag}}$ (green), DAPI-stained nucleoids (magenta), and phase-contrast (blue) in cells without (top) or with (bottom) McdA. Scale bar, 2 µm. (**E**) Proportion of cells with the indicated number of encapsulin foci from (D). (**F**) Pearson correlation coefficients measuring colocalization between encapsulin$^{\beta\text{-MapTag}}$ and nucleoids from

(D). (**G**) Super-resolution Airyscan images showing encapsulin$^{\beta\text{-MapTag}}$ (green) in cells without (top) or with (bottom) McdA. Scale bars, 2 µm. (**H**) Proportion of cells with the indicated number of encapsulin$^{\beta\text{-MapTag}}$ foci from (G).

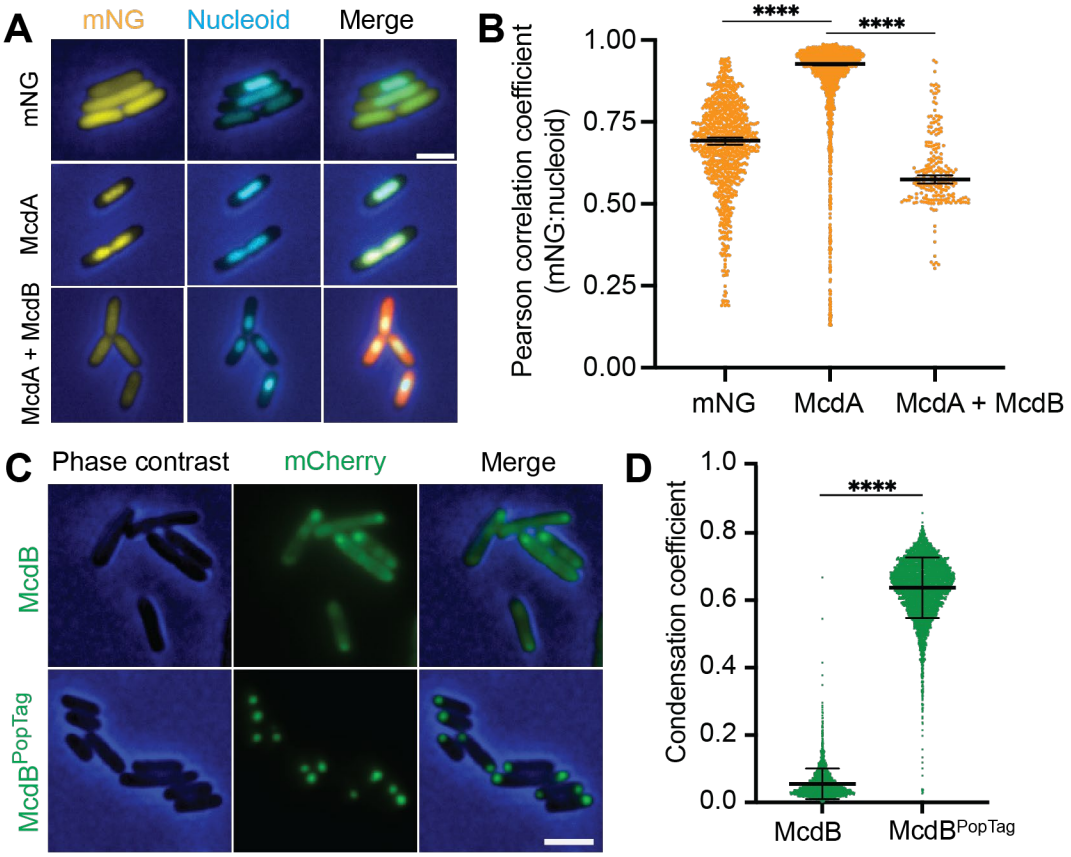

Supplementary Figure 3. McdB globally releases McdA from the *E. coli* nucleoid. (**A**) Wide-field fluorescence images of cells expressing mNeonGreen (mNG), mNG-McdA, or both mNG-McdA and mCherry-McdB. Channels shown are mNG (yellow), DAPI-stained nucleoids (cyan), phase-contrast (blue), and mCherry (red), acquired 2 hours post-induction following chloramphenicol (Cm, 100 µg/mL) treatment to condense the nucleoid. Merged images are provided. Scale bar, 2 µm. (**B**) Pearson correlation coefficients measuring colocalization of mNG, mNG-McdA, or mNG-McdA in the presence of mCherry-McdB with the DAPI-stained nucleoid. (**C**) Wide-field fluorescence images showing McdB (top) or McdB^{PopTag} (bottom) condensates in *E. coli*. Phase-contrast (blue) and mCherry (green) are shown, with merged images. Scale bar, 2 µm. (**D**) Single-cell condensation coefficients of McdB and McdB^{PopTag} from (C).

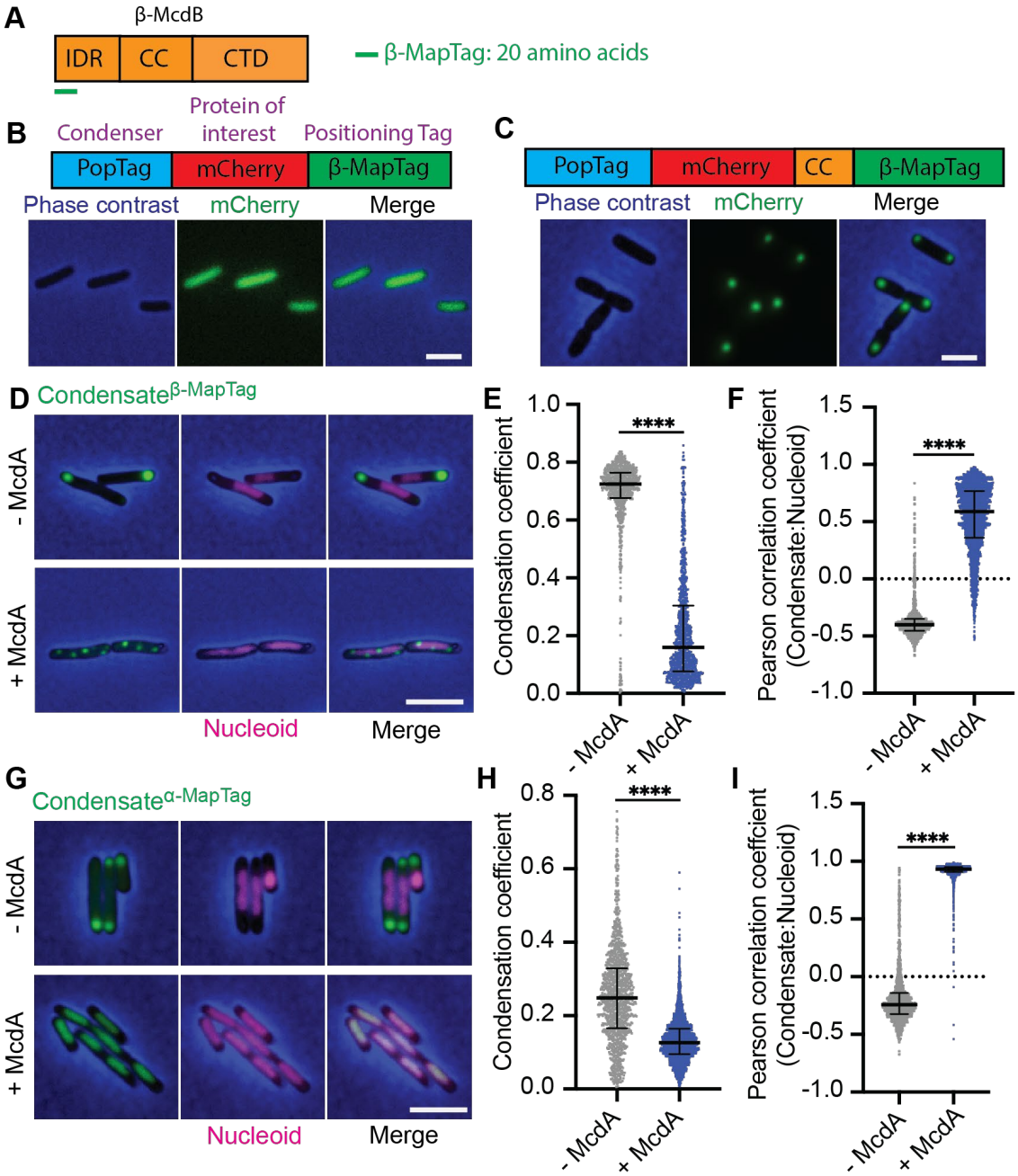

Supplementary Figure 4. McdA spatially organizes both α- and β-MapTagged condensate monomers on the *E. coli* nucleoid. (**A**) Schematic of β-McdB (from *S. elongatus*) domain organization: intrinsically disordered region (IDR, including the β-MapTag, first 20 amino acids), coiled-coil (CC) region, and C-terminal domain (CTD). (**B**) Wide-field fluorescence images showing that mCherry^{PopTag} fused to β-MapTag does not form condensates. Phase-contrast (blue), mCherry (green), and merged images are shown. Scale bar, 2 µm. (**C**) Addition of the CC region restores cytoplasmic condensate formation to mCherry^{PopTag}. (**D**, **G**) Wide-field fluorescence images of condensates fused to the β-MapTag (D) or α-MapTag (G), with condensates in green, DAPI-stained nucleoids in magenta, and phase-contrast in blue. Scale bars, 2 µm. (**E**, **H**) Single-cell condensation coefficients of proteins of interest fused to β-MapTag (E) or α-MapTag (H). (**F**, **I**) Pearson correlation coefficients for colocalization between proteins

of interest when fusing to β-MapTag (F) or α-MapTag (I) and DAPI-stained nucleoids.

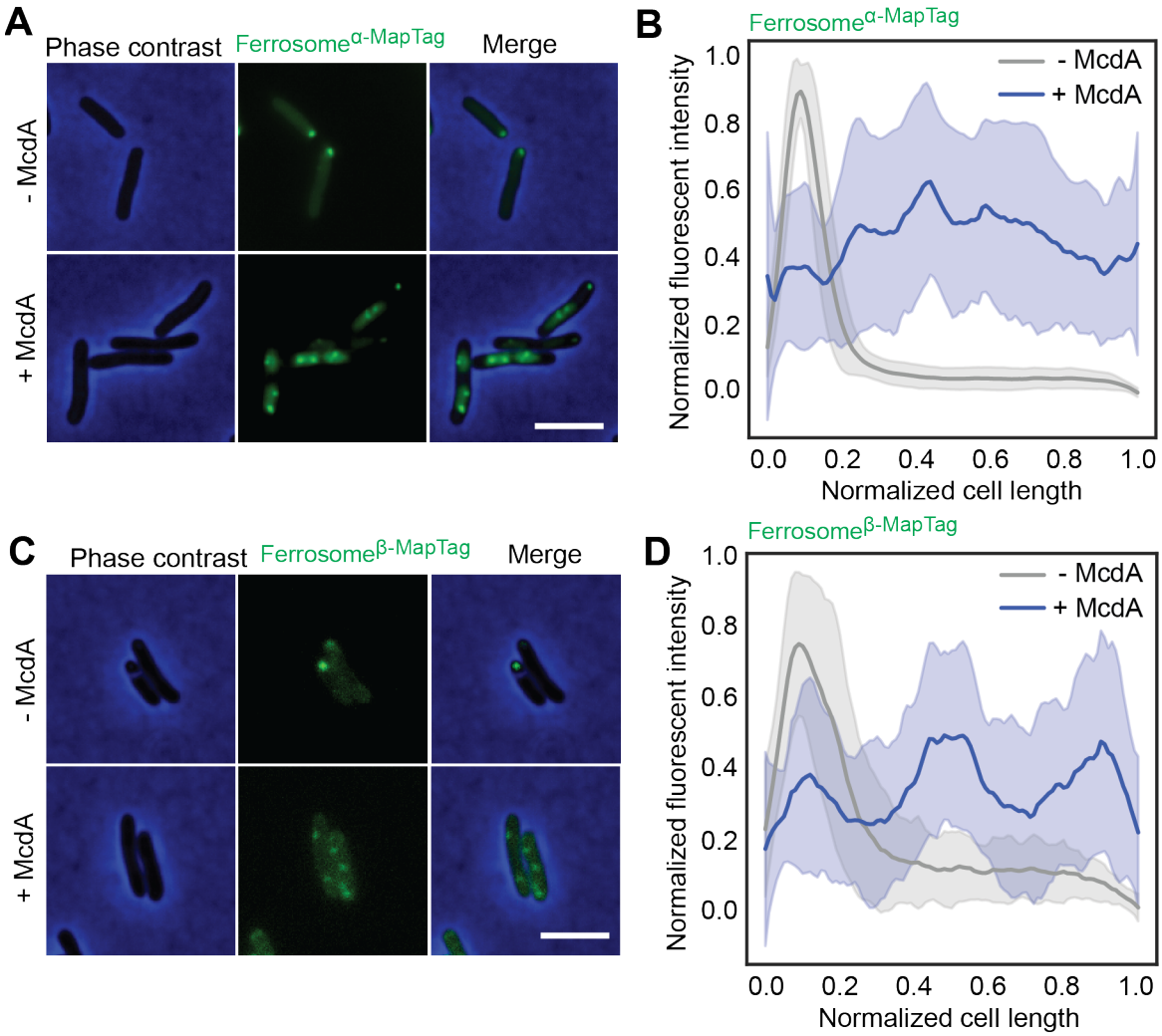

Supplementary Figure 5. McdA spatially organizes both α- and β- MapTagged ferrosomes on the *E. coli* nucleoid. (**A**, **C**) Wide-field fluorescence images of ferrosomes fused to the α-MapTag (A) or β-MapTag (C), with ferrosomes in green and phase-contrast in blue. Scale bars, 2 µm. (**B**, **D**) Fluorescence intensity profiles of ferrosome signals measured along the normalized cell length in cells containing ferrosome$^{\alpha\text{-MapTag}}$ (B) or ferrosome$^{\beta\text{-MapTag}}$ (D) foci.

Supplementary Table 1. Strains and plasmids used in this study

Strains & Plasmids	Description	Source
Strains		
E. coli Top10		
MG1655 Δ*lacY*		
Plasmids		
pDT074	Carboxysomes with CbbS C-terminally fused to mNeonGreen, Cm^R	(*4*)
pDT081	pDT074 + McdAB, Cm^R	This study
pDT075	Carboxysomes with CbbS C-terminally fused to mScarlet-I3, Cm^R	(*4*)
pDT082	pDT155 + McdAB, Cm^R	This study
pDT078	Carboxysomes with CbbS C-terminally fused to mJuniper, Cm^R	(*4*)
pDT084	pDT163 + McdAB, Cm^R	This study
pSMK1	Encapsulins with α-MapTag, Amp^R	This study
pYH84	P_{tet}- *mcdA* with *mcdA* from *H. neapolitanus*, Km^R	This study
pSMK2	Encapsulins with β-MapTag, Amp^R	This study
pYH91	P_{tet}- *mcdA* with *mcdA* from *S. elongatus*, Km^R	This study
pRED1	P_{tet}-*mNeonGreen*, Km^R	This study
pYH81	P_{tet}-*mNeonGreen-mcdA* with *mcdA* from *S. elongatus*, Km^R	This study
pYH71	P_{trc}-*mCherry-mcdB* with *mcdB* from *S. elongatus*, Amp^R	(*18*)
pYH82	P_{trc}-*mCherry-poptag-mcdB* with *mcdB* from *S. elongatus*, Amp^R	This study
pJAB30	P_{trc}-*mCherry-poptag-β-maptag*, Amp^R	This study
pJAB39	pJAB30 with added coiled-coil region	This study
pRED2	P_{trc}-*mCherry-poptag-α-maptag*, Amp^R	This study
pKM1	Ferrosomes with α-MapTag, Amp^R	This study
pKM2	Ferrosomes with β-MapTag, Amp^R	This study

Supplementary Table 2. Primers used in this study.

Primers	Description
oDT077	GTTGCCGCGGTAGACC
oDT098	GTCAAGTCTGTCATTGCGCTG
pSMK23-F	CAATTTCACACAGGAAACAGACC
pSMK2-R	CATGCCTGCAGGTCGACTCATCCCTCGCGAGCTATTGGGGTCCGTGAGCGCTTTTTAAGCCGGTCGAATGCATCCGTCATGCTGCCACC
KM1	CACAGGAAACAGACCATGGCAATGACGAACCTGGAGG
KM2	TATATAAAAATTCAAGCCGCTGCCCTTGTACAGCTCGTCCATGCCC
KM3	CTTATAACTACTATTAAATTCTAGAAATCTAAATGAAAGGATAATGTAAAATGAATATT
KM4	CTTGCATGCCTGCAGGTCGACTCATTATTCTGTTGTACAAGTATTATTT
KM5	CATGGACGAGCTGTACAAGGGCAGCGGCTTGAATTTTTATATAAAACACGAAATAAGAGG
KM6	CATTATCCTTTCATTTAGATTTCTAGAATTTAATAGTAGTTATAAGTATTGGTGTTTTCC
YH20	AGCTCCGCGACCACGCGAGA
YH21	TGAGTCGACCTGCAGGCATG
YH22	ATCTCGCGTGGTCGCGGAGCT GGATCCGGCAGCGGCAGC
YH23	CATGCCTGCAGGTCGACTCACCAACCGTGCAGCTTGCGT
YH24	CCCTTCACGGGCAATGGGAG
YH25	TGAGTCGACCTGCAGGCATG
YH26	ACGTTGTGCAATGGCCTCCT
YH27	TGAGTCGACCTGCAGGCATG

Supplementary Table 3. Reagents used in this study.

Reagent	Vendor	Catalog #	Use
Carbenicillin	Thermo Fisher Scientific	MT46100RG	To select for the plasmid in culture
Kanamycin	Sigma	K1377-5G	
Chloramphenicol	Sigma	C0378-100G	
DAPI	Thermo Fisher Scientific	D1306	To label the nucleoid
Glucose	Thermo Fisher Scientific	15023021	As a carbon source and to inhibit protein expression from the P_{trc} promoter
Glycerol	Thermo Fisher Scientific	G334	As a carbon source for *E. coli* MG1665
IPTG	Thermo Fisher Scientific	501126935	To induce protein expression
L-arabinose	Thermo Fisher Scientific	AC365181000	To induce protein expression
Anhydrotetracyclin			
Casamino acids	Millipore Sigma	65072-00-6	For AB medium
Thiamine	Millipore Sigma	T4625-5G	For AB medium
Uracil	Millipore Sigma	66-22-8	For AB medium
UltraPure agarose	Invitrogen	16500100	For agar pads
KasI	New England Biolabs	R0544S	Restriction enzyme
BamHI-HF	New England Biolabs	R3136S	Restriction enzyme
NcoI-HF	New England Biolabs	R3193S	Restriction enzyme
SalI-HF	New England Biolabs	R3138S	Restriction enzyme
QIAquick Gel Extraction Kit	QIAGEN	Q28704	Gel extraction
T4 DNA Ligase	New England Biolabs	M0202L	Cloning
NEBuilder HiFi DNA Assembly Master Mix	New England Biolabs	E2621L	Cloning
Phusion MM	New England Biolabs	M0531L	Cloning
QIAquick PCR Purification Kit	QIAGEN	28106	PCR purification

Supplementary Table 4. Statistical information from datasets in this study.

Figure	Experiment	N cells (N replicates)	Statistical Test
1C, D	Carboxysomes – mispositioned	344 (3)	Kolmogorov-Smirnov
	Carboxysomes – positioned	1514 (3)	
1F	Carboxysomes – mispositioned over time	3246 (3)	
1H	Carboxysomes – positioned over time	8942 (3)	
2C	Encapsulins – mispositioned & positioned	1759 (3) + 937 (3)	Kolmogorov-Smirnov
2D	Encapsulins – mispositioned & positioned	1759 (3) + 937 (3)	
2F	Encapsulins – mispositioned over time	780 (3)	
2H	Encapsulins – positioned over time	345 (3)	
2J	Encapsulins – McdA removal	1080 (3)	
2L	Encapsulins – McdA addition	369 (3)	
3C	Condensates – mispositioned & positioned	20 (3) + 20 (3)	
3D	Condensates – mispositioned & positioned	1423 (3) + 1872 (3)	
3J	Condensates – McdA removal	17555 (3)	
3L	Condensates – McdA addition	625 (3)	
4C	Ferrosomes – mispositioned & positioned	179 (3) + 197 (3)	Kolmogorov-Smirnov
4D	Ferrosomes – mispositioned & positioned	179 (3) + 197 (3)	
4F	Ferrosomes – positioned over time	3439 (3)	
4H	Ferrosomes – McdA addition	2676 (3)	

Supplementary Table 5. Detection parameters for image analysis

Experiment	Threshold	Min sigma	Max sigma	Overlap	Denoise radius/ blur radius	Denoise amount	Tolerance	Figure
Carboxysomes Mispositioned	0.007	2.5	3	0.5	2	3	-	1C, D
Carboxysomes Positioned	0.01	2.5	3	0.75	1	-	1.5	1C, D
Encapsulins Mispositioned (Hn)	0.04	0.75	2.5	0.05	1	6	-	2C, D
Encapsulins Positioned	0.025	0.75	2.5	0.05	1	6	–	2C, D
Encapsulins Mispositioned (Se)	100	2.5	3	0.25	1	-	1.5	S2D
Encapsulins McdA removal	25	2.5	3	0.25	1	-	1.5	2J
Encapsulins McdA addition	100	2.5	3	0.25	1	-	1.5	2L
Condensates Mispositioned	0.05	2.5	3	0.5	2	3	-	3D
Condensates Positioned	0.03	2.5	3	0.5	2	3	-	3D
Condensates McdA removal	0.005	2.5	3	0.5	2	3	-	3J
Condensates McdA addition	0.005	2.5	3	0.5	2	3	-	3L

Video S1. The McdAB system spatially organizes carboxysomes on the *E. coli* nucleoid. Time-lapse wide-field fluorescence microscopy of cells with (left) and without (right) the McdAB system. mNG-labeled carboxysomes are shown in green and phase-contrast in blue. Scale bar, 5 μm.

Video S2. The McdAB system regulates both assembly and positioning of carboxysomes in *E. coli*. *In situ* cryo-electron tomography of *E. coli* cells without (left) or with (right) the McdAB system. Carboxysomes are shown in green, Rubisco in pink, ribosomes in yellow, and the cell membrane in blue.

Video S3. McdA distributes MapTagged encapsulins on the *E. coli* nucleoid. Time-lapse wide-field fluorescence microscopy of cells with (left) and without (right) McdA. mNG-labeled encapsulins are shown in green and phase-contrast in blue; scale bars, 5 μm.

Video S4. Reversible control of encapsulin positioning by McdA manipulation. Time-lapse wide-field fluorescence microscopy shows encapsulin positioning in response to McdA removal (left) or addition (right). mNG-labeled encapsulins are shown in green and phase-contrast in blue. Scale bars, 2 μm.

Video S5. McdA distributes McdB^{PopTag} condensates on the *E. coli* nucleoid. Time-lapse wide-field fluorescence microscopy of cells with (left) and without (right) McdA. Condensates are shown in green and phase-contrast in blue. Scale bars, 5 μm.

Video S6. Reversible control of McdB^{PopTag} condensate positioning by McdA manipulation. Time-lapse wide-field fluorescence microscopy shows encapsulin positioning in response to McdA removal (left) or addition (right). Condensates are shown in green and phase-contrast in blue. Scale bars, 5 μm.

References

1. W. Bonacci, P. K. Teng, B. Afonso, H. Niederholtmeyer, P. Grob, P. A. Silver, D. F. Savage, Modularity of a carbon-fixing protein organelle. *Proceedings of the National Academy of Sciences of the United States of America* **109**, 478–483 (2012).

2. T. W. Giessen, B. J. Orlando, A. A. Verdegaal, M. G. Chambers, J. Gardener, D. C. Bell, G. Birrane, M. Liao, P. A. Silver, Large protein organelles form a new iron sequestration system with high storage capacity. *eLife* **8**, e46070 (2019).

3. Y. Dai, M. Farag, D. Lee, X. Zeng, K. Kim, H. Son, X. Guo, J. Su, N. Peterson, J. Mohammed, M. Ney, D. M. Shapiro, R. V. Pappu, A. Chilkoti, L. You, Programmable synthetic biomolecular condensates for cellular control. *Nat Chem Biol* **19**, 518–528 (2023).

4. D. S. Trettel, Y. Hoang, A. G. Vecchiarelli, C. R. Gonzalez-Esquer, Robust Synthetic Biology Toolkit to Advance Carboxysome Study and Redesign. *ACS Synth. Biol.* **14**, 2219–2229 (2025).

5. L. T. Pulianmackal, J. M. I. Limcaoco, K. Ravi, S. Yang, J. Zhang, M. K. Tran, M. Ghalmi, M. J. O'Meara, A. G. Vecchiarelli, Multiple ParA/MinD ATPases coordinate the positioning of disparate cargos in a bacterial cell. *Nat Commun* **14**, 3255 (2023).

6. D. F. Savage, B. Afonso, A. H. Chen, P. A. Silver, Spatially Ordered Dynamics of the Bacterial Carbon Fixation Machinery. *Science* **327**, 1258–1261 (2010).

7. J. S. Maccready, P. Hakim, E. J. Young, L. Hu, J. Liu, K. W. Osteryoung, A. G. Vecchiarelli, D. C. Ducat, Protein gradients on the nucleoid position the carbon-fixing organelles of cyanobacteria. *eLife* **7** (2018).

8. J. S. MacCready, A. G. Vecchiarelli, Positioning the Model Bacterial Organelle, the Carboxysome. *mBio* **12**, e02519-19 (2021).

9. R. Rillema, Y. Hoang, J. S. MacCready, A. G. Vecchiarelli, Carboxysome Mispositioning Alters Growth, Morphology, and Rubisco Level of the Cyanobacterium Synechococcus elongatus PCC 7942. *mBio* **12**, e02696-20 (2021).

10. A. Occhialini, M. T. Lin, P. J. Andralojc, M. R. Hanson, M. A. J. Parry, Transgenic tobacco plants with improved cyanobacterial Rubisco expression but no extra assembly factors grow at near wild-type rates if provided with elevated CO2. *Plant Journal* **85**, 148–160 (2016).

11. Y. Fang, F. Huang, M. Faulkner, Q. Jiang, G. Dykes, M. Yang, L.-N. Liu, Engineering and modulating functional cyanobacterial CO_2-fixing organelles. *Frontiers* **9** 10.3389/fpls.2018.00739 (2018).

12. L. M. Oltrogge, A. W. Chen, T. Chaijarasphong, J. B. Turnšek, D. F. Savage, α-Carboxysome Size Is Controlled by the Disordered Scaffold Protein CsoS2. *Biochemistry* **63**, 219–229 (2024).

13. Tuning the interaction of a ParA-type ATPase with its partner separates bacterial organelle positioning from partitioning | bioRxiv. https://www.biorxiv.org/content/10.1101/2025.05.22.655647v1.

14. T. W. Giessen, Encapsulins. *Annu Rev Biochem* **91**, 353–380 (2022).

15. J. M. Flynn, I. Levchenko, M. Seidel, S. H. Wickner, R. T. Sauer, T. A. Baker, Overlapping recognition determinants within the ssrA degradation tag allow modulation of proteolysis. *Proceedings of the National Academy of Sciences* **98**, 10584–10589 (2001).

16. C. A. Azaldegui, A. G. Vecchiarelli, J. S. Biteen, The emergence of phase separation as an organizing principle in bacteria. *Biophysical Journal* **120**, 1123–1138 (2021).

17. D. M. Mitrea, M. Mittasch, B. F. Gomes, I. A. Klein, M. A. Murcko, Modulating biomolecular condensates: a novel approach to drug discovery. *Nat Rev Drug Discov* **21**, 841–862 (2022).

18. Y. Hoang, C. A. Azaldegui, R. E. Dow, M. Ghalmi, J. S. Biteen, A. G. Vecchiarelli, An experimental framework to assess biomolecular condensates in bacteria. *Nat Commun* **15**, 3222 (2024).

19. K. Lasker, S. Boeynaems, V. Lam, D. Scholl, E. Stainton, A. Briner, M. Jacquemyn, D. Daelemans, A. Deniz, E. Villa, A. S. Holehouse, A. D. Gitler, L. Shapiro, The material properties of a bacterial-derived biomolecular condensate tune biological function in natural and synthetic systems. *Nat Commun* **13**, 5643 (2022).

20. H. Pi, R. Sun, J. R. McBride, A. R. S. Kruse, K. N. Gibson-Corley, E. S. Krystofiak, M. R. Nicholson, J. M. Spraggins, Q. Zhou, E. P. Skaar, Clostridioides difficile ferrosome organelles combat nutritional immunity. *Nature* **623**, 1009–1016 (2023).

21. T. S. Lee, R. A. Krupa, F. Zhang, M. Hajimorad, W. J. Holtz, N. Prasad, S. K. Lee, J. D. Keasling, BglBrick vectors and datasheets: A synthetic biology platform for gene expression. *J Biol Eng* **5**, 12 (2011).

22. S. K. Govers, J. Mortier, A. Adam, A. Aertsen, Protein aggregates encode epigenetic memory of stressful encounters in individual escherichia coli cells. *PLoS Biology* **16**, e2003853 (2018).

23. alisterburt, D. Tegunov, tegunovd, M. Wachsmuth-Melm, warpem/warp: v2.0.0dev33, Zenodo (2025); https://doi.org/10.5281/zenodo.14977238.

24. L. Lamm, S. Zufferey, R. D. Righetto, W. Wietrzynski, K. A. Yamauchi, A. Burt, Y. Liu, H. Zhang, A. Martinez-Sanchez, S. Ziegler, F. Isensee, J. A. Schnabel, B. D. Engel, T. Peng, MemBrain v2: an end-to-end tool for the analysis of membranes in cryo-electron tomography. bioRxiv [Preprint] (2024). https://doi.org/10.1101/2024.01.05.574336.